Flow Measurements in a Suction Sump by UVP

Katsuya Hirata, Masakatsu Hattori, Masashi Neya and Jiro Fuanaki.
Dept. Mech. Engng., Doshisha Univ., Kyoto 610-0321, Japan

Hiroya Tanigawa
Dept. Mech. Engng., National College of Technology, Maizuru 625-8511, Japan

In the present study, to reveal the air entrainment mechanism into a suction pipe in a suction sump, the authors conduct flow-velocity measurements by UDM (Ultrasonic Doppler Method). Here, we consider the simplest geometry as a suction sump, that is, a straight channel with rectangle-cross section and a simple suction pipe near the end of the channel. Ultrasonic transducers are fixed outside the side, bottom and back walls with near-right angle and, we get three-dimensional time-mean velocity distributions and equi-vorticity contours. At first, measurement accuracy is checked by comparing velocity profiles by UDM with hydrogen bubble method. As a result, the authors show typical flow fields in the sump, and show the relation between flow pattern and air entrainment. Especially, we compare two cases where the air entrainment is often observed.

Keywords: suction sump, open sump, two-phase flow, vortex, pump, water tank

1 INTRODUCTION

In power generation plants, irrigations, drainages, and so on, the optimum designs of suction sumps are needed to get low cost, compact size and high efficiency. As well, in resent years, we often require miniaturization of suction sumps. In such situations, the air entrainment often induces vibrations and noises, which may result in pump's low efficiency or collapse, or which may stop water-vein managements of rivers (for example, see reference [1]).

Hirata et al [2] have conducted series of air entrainment experiments, and revealed the critical conditions to occur the air entrainment. However, fore precise prediction of the air entrainment, we have to understand the flow field in the sump accurately and in detail.

Concerning the flow in the sump, Tagomori and Ueda [3] carried out qualitative observations, namely, flow visualization using aluminum flakes or polyethylene particles. Constantinescu and Patel [4] carried out three-dimensional numerical simulations with a k-ε turbulent model, and reveal a steady flow field at a Reynolds number of 60000.

Till now, there is no quantitative observation on actual flow in the sump. Then, in the present study, we show velocity vectors and vorticity contours using an ultrasonic-velocity-profile monitor [5] (hereafter, refereed to as UVP), and reveal the time-mean three-dimensional flow structures. Specifically speaking, we study two cases, that is, cases A and B. In both cases, we often observe the air entrainment from a free surface into the suction pipe. In the case A, we see two air strings, whose position is in the leeward of the suction pipe with small fluctuation. In the case B, we see the air entrainment from anywhere on the circumference of the suction pipe. The position where the air entrainment occurs is unstable in random manner.

2 EXPERIMENTAL METHOD

2.1 Experimental apparatus

Figure 1 shows the present model, that is, a suction sump and a suction pipe with the simplest geometries. And, table 1 shows basic dimensions of the model. Tested cases are two, cases A and B. The difference between two cases is only Z/D. Here, D is the outer diameter of the suction pipe, and is used as a length scale. A velocity scale is the mean flow velocity V_b at the bell-mouth-type intake of the suction pipe, which is defined as

$$V_b=4Q/(\pi D^2) \quad (1)$$

where Q is the flow rate into the suction pipe.

Table 1 shows governing kinetic parameters, as well. As the Froude number is the most important parameter, we show the value calculated using another definition where a velocity scale is the mean velocity U_c at a cross section of the sump channel, for reference.

Figure 2 shows a schematic diagram of the present

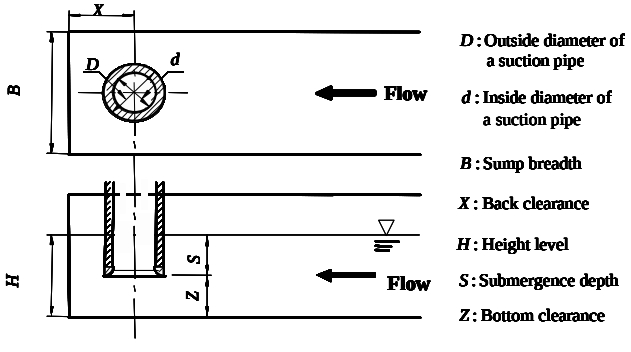

Figure1: Suction sump and suction pipe

Table1: Experimental parameters

	Case A	Case B
D [mm]	38	←
d [mm]	34	←
B/D	3.16	←
X/D	1.58	←
Z/D	0.39	1.18
H/D	1.58	←
V_b [m/s]	0.6	←
U_c [m/s]	0.095	←
$Fr=V_b/(gD)^{0.5}$	0.98	←
$Fr(U_c)=U_c/(gD)^{0.5}$	0.156	←
$Re=V_bD/v$	2.2×10^4	←
$Bo=\rho_w gD^2/\sigma$	200	←
$We=V_b(\rho_w D/\sigma)^{0.5}$	14	←

experimental apparatus. A pump B (No.2 in the figure) feed working fluid (water) to a suction sump (No.9) from a reservoir tank. We control the flow rate from the pump A by a control valve, and then control the water level in the suction sump. At the upstream of the suction sump, namely, at 0.84 [m] upstream from the back wall of the suction sump, we put a strainer (No.10) to get a uniform flow. The strainer consists of unwoven fabric sandwiched between two wire meshes with diameter of 0.001 [m] and gap of 0.001 [m]. A bend-type jet pump (No.6 and 7) pump up water in the suction sump into the suction pipe (No.8). Here, the jet pump has less swirling component, than ordinary pumps. The jet pump is driven by a pump A (No.1). We measure its primary flow rate using an electro-magnetic flow meter (No.3, 4 and 5). And, we measure the total sum of the primary and secondary flow using a triangle weir (No.12). Water from the weir falls into the reservoir tank, then, a water-circulation system is closed. We measure velocities in the suction sump using a UVP monitor (No.11) through side walls, a bottom wall or a back wall.

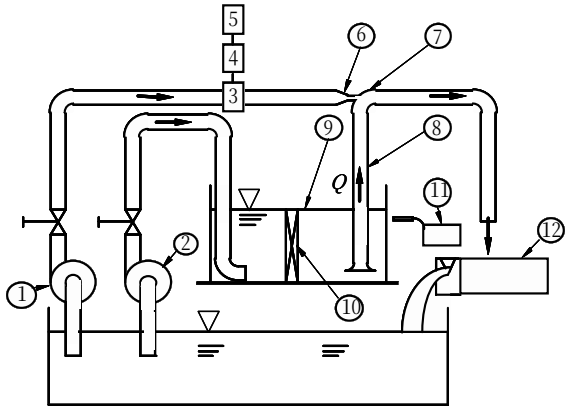

1. Turbo pump A
2. Turbo pump B
3. Electro Magnetic Flow Meter
4. Converter
5. Digital multi meter
6.Nozzle
7. Bend-type jet pump
8. Suction pipe
9. Suction sump
10. Filter
11. UVP monitor
12. Triangle weir

Figure 2: Schematic of experimental apparatus

2.2 Velocity measurements by UVP monitor

In the present study, the number of measuring points is 128 in one profile, and then, the space resolution on the profile is 0.75 [mm]. As the diameter of the ultrasonic beam is 5 [mm], one measuring volume is a disc with a diameter of 5 [mm] and with a thickness of 0.75 [mm]. We get consecutive 1024 profiles at each measurement with an interval of 32 [ms] or more.

When we get time mean velocities, we average more than 200 profiles, which is enough for the present cases, as the present flow is almost steady with weaker turbulence. Owing to the air entrainment, there often exist free surfaces under the mean water level. As accurate UVP measurements are impossible near free surfaces, we avoid such measurements.

Tracer is polyethylene particle with a mean diameter of 1.2×10^{-5} [m]. As the particle's density lighter than water (its specific gravity is 0.918), we coat particles with surface-active agent to be suspended into water.

Figure 3 shows the definition of the present coordinate system. At each measurement point in the suction sump, we get three velocity components u, v and w.

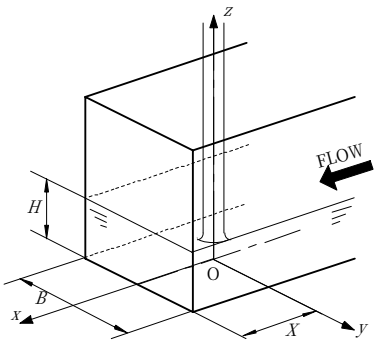

Figure 3: Definition diagram for coordinate system

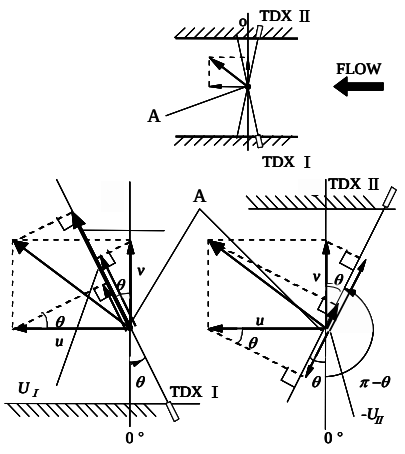

Figure 4: Definition diagram for measurements by UVP

Especially at the upstream of the suction sump, it becomes difficult to get fine measurements, as such place is far from the back wall. For example, when we get u components at a point A, we measure two velocities U_{I} and U_{II} as shown in figure 4. Then we calculate u according to the following.

$$u=(U_{\mathrm{I}}+U_{\mathrm{II}})/2\sin\theta \qquad (2)$$

In the present, transducer's tilting angle θ is fixed to 10°.

3 RESULTS AND DISCUSSION

3.1 Accuracy check

In order to confirm the accuracy of velocity measurements, we compare a UVP result with a time line by the hydrogen bubble method. Figure 5 shows a comparison between velocity distributions by two methods for the same channel flow. As a result, we can confirm good agreement as shown in figure 5.

3.2 Case A

Now we show some typical results for the case A. Figure 6 shows velocity vectors and vorticity contours on the *x*-*y* plane at *z*/*D*=0.95 (near free surface). Flow is almost symmetrical concerning the centre line *y*/*D*=0. And, there is a pair of swirls with the opposite rotation. The position of these swirls' centre almost coincide with the positions of two string-like air bulks accompanied with the air entrainment from the atmosphere into the suction pipe.

Figure 7 shows velocity vectors and vorticity contours on the *y*-*z* plane at *x*/*D*=-1.58 (upstream of the suction pipe). As well as figure 6, flow is almost symmetrical concerning the centre line *y*/*D*=0. And, we can see a pair of swirls with the opposite rotation, which is longitudinal vortex pair with stream wise axis.

Figure 8 shows velocity vectors and vorticity contours on the *x*-*z* plane at *y*/*D*=-0.63 (in front of th suction sump). At *x*/*D* 0.2, there is a strong downward flow. Besides, in the downstream of the suction sump, we can see a swirl with anti-clockwise strong vorticity. This swirl centre also coincides with the position of the string-like air bulk.

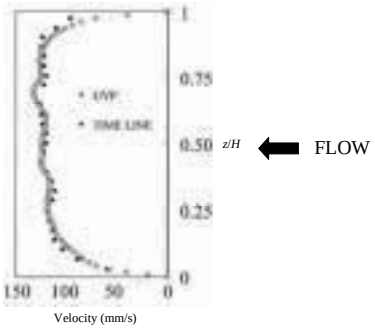

Figure 5: Calibration of UVP by hydrogen bubble method

3.2 Case B

Next, we show some typical results for the case B. Here, flow in the case B strongly fluctuates with time, and the flow symmetry about the sump centre is frequently and randomly broken. So, in order to make the flow almost steady, we slightly tilt the upstream strainer. In such condition, mean velocity on the positive *y* side is a little bit faster than the negative *y* side.

Figure 9 shows velocity vectors on the *x*-*y* plane at *z*/*D*=0.63 (near the sump bottom below the suction pipe). We can see only one swirl on the negative *y* side in the downstream of suction pipe. Such clear swirl exists not on the *x*/*y* plane near or above the suction intake, but on the *x*/*y* plane below the intake.

Figure 10 shows velocity vectors on the *y*-*z* plane at *x*/*D*=0.63 (leeward of the suction pipe). We can see only one swirl with anti-clockwise vorticity in the negative *y* side.

Figure 11 shows velocity vectors on the *x*-*z* plane at *y*/*D*=0.47 (behind the suction pipe). In the downstream of the suction pipe near the free surface, we ca see reversed flow, corresponding to a complicated three-dimensional flow structure.

In summary, the case B is in the category "[6] column vortex" in the conventional classification. If we consider the flow structure under the free surface, the case B is not properly characterized by the concentric flow around the suction pipe axis.

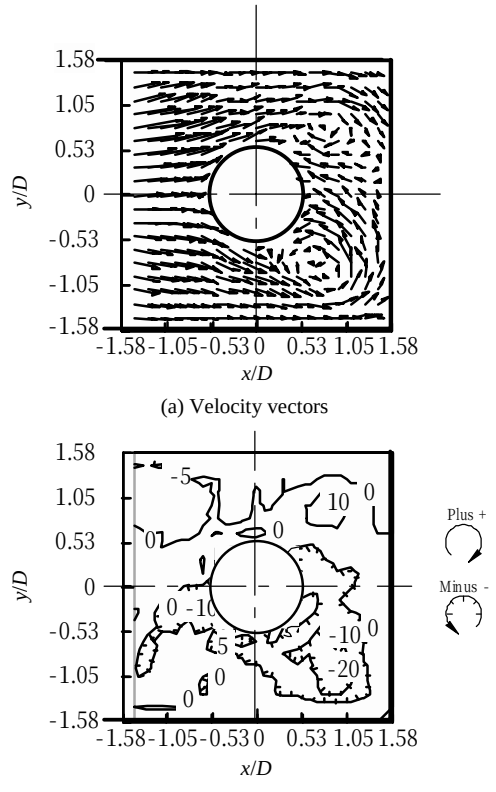

Figure 6: Velocity vectors and vorticity contours on the *x*-*y* plane at *z*/*D*=0.95 (case A)

4 CONCLUSIONS

We have conducted UVP measurements in a suction sump, and revealed the mean three-dimensional flow structures quantitatively. Both tested cases have complicated flow structures under the free surface, which are difficult to be expected only from surface observations.

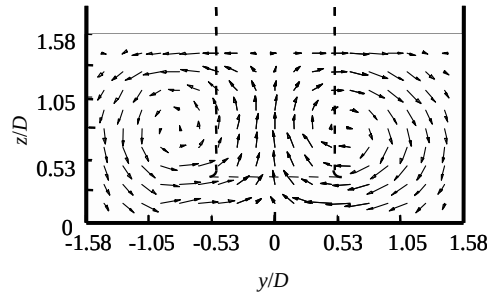

(a) Velocity vectors

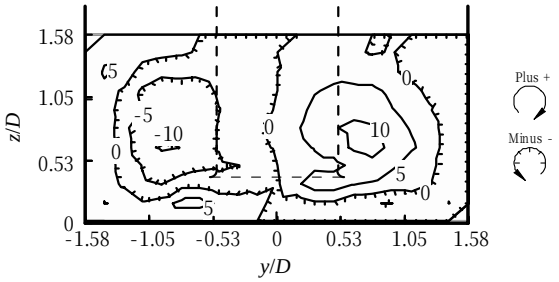

(b) Vorticity contours [s^{-1}]

Figure 7: Velocity vectors and vorticity contours on the *y*-*z* plane at *x*/*D*=-1.58 (case A)

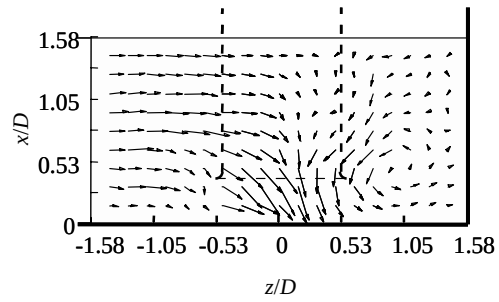

(a) Velocity vectors

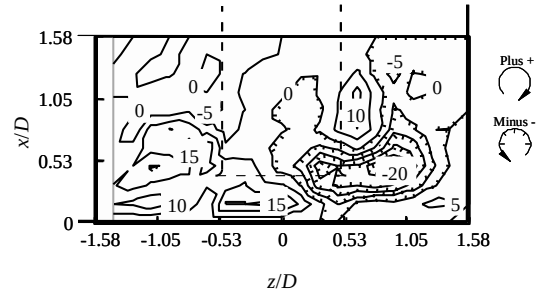

(b) Vorticity contours [s^{-1}]

Figure 8: Velocity vectors and vorticity contours on the *x*-*z* plane at *y*/*D*=-0.63 (case A)

REFERENCES

[1] JSME standard, standard method for model testing the performance of a pump sump, JSME S 004 (1984) (in Japanese).

[2] Katsuya H., Jiro F. and Masashi N.: On the critical submergence for air entraining vortices in a suction sump, JSCE Journal of Hydraulic, Coastal and Environmental Engineering, Vol.65 No.747 (2003) 61-69 (in Japanese).

[3] Masashi T. and Haruo U.: An experimental study on submerged vortices and flow pattern in the pump sump, Transaction of JSME, series B, Vol.57 No. 543 (1991) 3641-3646 (in Japanese).

[4] G. S. Constantinescu and V. C. Patel: Numerical model for simulation of pump-intake flow and vortices, Journal of Hydraulic Engineering, Vol.4 No.2 (1998) 123-134.

[5] Yasushi T.: Velocity profile measurement by ultrasound Doppler shift method, Int. J. Heat and Mass Flow, Vol.7 (1986) 313-318 (in Japanese).

[6] H. W. Iversen: Studies of submergence requirements of high-specific-speed pumps, Transaction of ASME, Vol.75 (1953)635-641.

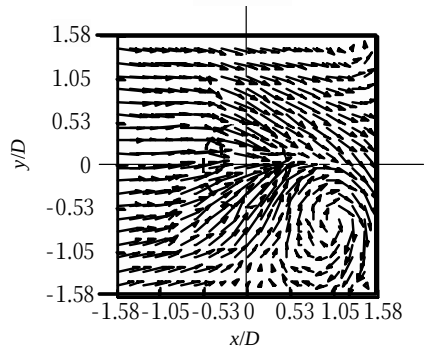

Figure 9: Velocity vectors on the *x*-*y* plane at *z*/*D*=0.63 (case B)

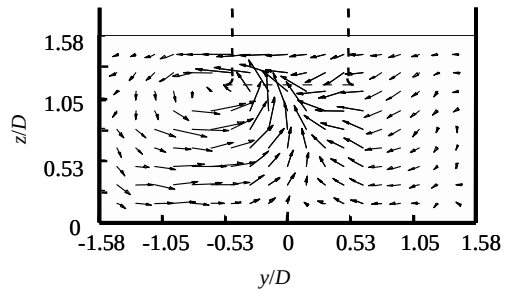

Figure 10: Velocity vectors on the *y*-*z* plane at *x*/*D*=0.63 (case B)

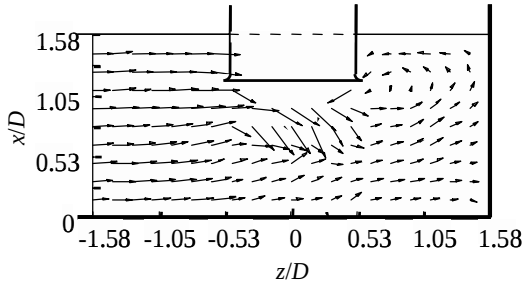

Figure 11: Velocity vectors on the *x*-*z* plane at *y*/*D*=0.47 (case B)